FREE VIBRATION ANALYSIS OF PLANE STRESS/STRAIN MODELS USING KRIGING-BASED FINITE ELEMENT METHOD

Christiana[1] dan Wong Foek Tjong[2]
[1] Student of Master Program in Civil Engineering, Petra Christian University, Surabaya
[2] Assoc. Prof., Department of Civil Engineering, Universitas Kristen Petra, Surabaya

[1] b21220001@john.petra.ac.id, [2] wftjong@petra.ac.id

ABSTRACT: Kriging-based finite element method (K-FEM) is an enhancement of standard FEM that employs Kriging interpolation over nodal points both within and outside the element domain. This method significantly increase the accuracy of conventional FEM. This paper presents the development and applications of the K-FEM to free vibration analysis of plane bodies with negligible damping. Six benchmark problems are examined: a cantilever beam, a simply supported beam, an arch, a shear wall, a slope, and a tapered cantilever plate with a hole. The computed natural frequencies and mode shapes demonstrate close agreement with reference solutions. Convergence toward the reference values is achieved as the mesh is refined and the degree of the polynomial basis increases, while additional DOI layers exert only a minor influence. These findings confirm that K-FEM is a viable alternative to the conventional FEM for free vibration analysis of plane stress and plane strain models.

Keywords: free vibration, Kriging-based finite element, plane stress, plane strain, natural frequency, mode shape

1. INTRODUCTION

The finite element method (FEM) is a numerical method that can solve a wide variety of complex engineering and scientific problems. FEM has been applied in various engineering fields for the design of buildings, machines, ships, planes, and so on (Cook *et al.*, 2002). The popularity of the FEM is because this method can be easily applied with computer programs (Kim, 2014). However, it cannot be denied that FEM has a low level of accuracy on linearly ordered isoparametric elements, which are highly dependent on the meshing process (Lee & Bathe, 1993) and cannot accurately solve problems with a Poisson's ratio close to 0.5 (Coombs *et al.*, 2018).

To overcome the weaknesses of the FEM, it is necessary to enhance the standard FEM. In this study, an enhanced FEM with Kriging interpolation (K-FEM) (Wong & Kanok-Nukulchai, 2009) is considered. The K-FEM is a type of FEM with the trial function interpolating nodes within and around the elements being considered. The interpolation function in this method is constructed "element-by-element" so that it is not continuous along the boundaries between elements. Although the K-FEM interpolation function is not continuous, K-FEM is proven to be a method that has good convergence properties. In addition, K-FEM also has the advantage that high-order polynomial basis functions can be included in elements

without requiring additional nodes in elements (Wong & Kanok-Nukulchai, 2009; Wong *et al.*, 2016).

In the application to plane elasticity problems, the K-FEM has been extensively tested in static problems (Wong & Kanok-Nukulchai, 2009; Wong *et al.*, 2016). Therefore, this study aims to develop the K-FEM for free vibration analysis of plane stress and plane strain models. Firstly, the K-FEM formulation and computer codes for linear static analysis of plane elasticity models were extended to include the mass matrix and eigenvalue solution. After that, numerical tests on six plane elasticity problems were conducted. The problems include a cantilever beam, a simply-supported beam, a thick arch, a shear wall, a slope, and a tapered cantilever plate with a hole.

2. KRIGING-BASED FINITE ELEMENT METHOD

2.1 Kriging Interpolation

Kriging interpolation is a geostatistical technique for space interpolation that is widely used in geology and mining, where the name Kriging is taken from the name of a South African mining engineer named Danie G. Krige (Plengkhom and Kanok-Nukulchai, 2005; Gu, 2003; Olea, 2012). The use of Kriging interpolation aims to find the unknown value at a point by interpolating several values around that point.

In the context of the K-FEM, Kriging interpolation within a typical finite element is constructed based on the nodal points within and outside of the element. Nodal points outside the element may include nodal points in the first, second, or more layers surrounding the element being considered. The area that includes all the points used in constructing the interpolation function forms layers around the elements, which is referred to as the domain of influencing nodes (DOI). Kriging interpolation calculations require a polynomial basis function and a correlation function. Polynomial basis functions can use a linear, quadratic, or higher degree polynomial, and correlation functions can use a Gaussian correlation function.

In a domain Ω under consideration, there are several sampling points $\mathbf{x}_\mathrm{i}$ where i=1, 2, …, N where N is the total number of nodes in the domain. Let $u(\mathbf{x})$ be the unknown field variable. The given data is the function values at the sampling points, that is, $u(\mathbf{x}_1), u(\mathbf{x}_2), \dots, u(\mathbf{x}_\mathrm{n})$. We seek the value of $u(\mathbf{x}_0)$, $\mathbf{x}_0$ is any point in Ω other than the sampling points. Let points $\mathbf{x}_1, \mathbf{x}_2, \dots, \mathbf{x}_n$ are some sampling points surrounding point $\mathbf{x}_0$ (in the DOI of $\mathbf{x}_0$). Then, the value of $u(\mathbf{x_0})$ can be interpolated from the values of $u(\mathbf{x}_1), u(\mathbf{x}_2), \dots, u(\mathbf{x}_\mathrm{n})$. Kriging estimates the value $u^h(\mathbf{x}_0)$ as a linear combination of $u(\mathbf{x}_1), u(\mathbf{x}_2), \dots, u(\mathbf{x}_\mathrm{n})$, so it can be written as follows (Wong & Kanok-Nukulchai, 2009):

$$u^h(\mathbf{x}_0) = \sum_{\mathrm{i}=1}^{\mathrm{n}} w_\mathrm{i} u(\mathbf{x}_\mathrm{i}) \quad (1)$$

where:

w_i : Kriging weight.

n : number of nodes in the DOI.

The value of the function $u(\mathbf{x})$is the realization of the random function $U(\mathbf{x})$, so Eq. 1 can be written as follows:

$$u^h(\mathbf{x}_0) = \sum_{i=1}^{n} w_i U(\mathbf{x}_i) \quad (2)$$

Kriging weights on the estimated value $U^h(\mathbf{x}_0)$ are unbiased, and the variance of the error from the estimated value must be minimum. These two conditions are written as follows:

$$\mathrm{E}[U^h(\mathbf{x}_0) - U(\mathbf{x}_0)] = 0 \quad (3)$$

$$\mathrm{var}[U^h(\mathbf{x}_0) - U(\mathbf{x}_0)] = 0 \quad (4)$$

Using the Lagrange method for a constraint optimization problem, the requirements for unbiased weights and minimum variance lead to the Kriging equation as follows (Ludong *et al.*, 2018):

$$\mathbf{R}\mathbf{w} + \mathbf{P}\boldsymbol{\mu} = \mathbf{r}(\mathbf{x}_0) \quad (5)$$

$$\mathbf{P}^{\mathrm{T}}\mathbf{w} = \mathbf{p}(\mathbf{x}_0) \quad (6)$$

where:

$$\mathbf{R} = \begin{bmatrix} C(\mathbf{h}_{11}) & \dots & C(\mathbf{h}_{1n}) \\ \dots & \dots & \dots \\ C(\mathbf{h}_{n1}) & \dots & C(\mathbf{h}_{nm}) \end{bmatrix}; \mathbf{P} = \begin{bmatrix} p_1(\mathbf{x}_1) & \dots & p_m(\mathbf{x}_1) \\ \dots & \dots & \dots \\ p_1(\mathbf{x}_n) & \dots & p_m(\mathbf{x}_n) \end{bmatrix} \quad (7)$$

$$\mathbf{w} = [w_1 \quad \dots \quad w_n]^{\mathrm{T}}; \boldsymbol{\mu} = [\mu_1 \quad \dots \quad \mu_m]^{\mathrm{T}} \quad (8)$$

$$\mathbf{r}(\mathbf{x}_0) = [C(\mathbf{h}_{10}) \quad C(\mathbf{h}_{20}) \quad \dots \quad C(\mathbf{h}_{n0})]^{\mathrm{T}}; \mathbf{p}(\mathbf{x}_0) = [p_1(\mathbf{x}_0) \quad \dots \quad p_m(\mathbf{x}_0)]^{\mathrm{T}} \quad (9)$$

where:

R : dimensionless covariance matrix n x n.
P : polynomial matrix at dimension points n x m.
w : dimensionless Kriging weight vector n x 1.
μ : vector multiplier of Lagrange dimension m x 1.
$\mathbf{r}(\mathbf{x}_0)$: covariance vector between the points and the point being searched for has dimension n x 1.
$\mathbf{p}(\mathbf{x}_0)$: polynomial basis vector at point $\mathbf{x}_0$.
$C(\mathbf{h}_{ij})$: cov $[U(\mathbf{x}_i), U(\mathbf{x}_j)]$= covariance function value between point random i and j.
h_{ij} : $h_i - h_j$= the distance between the point $\mathbf{x}_i$ and $\mathbf{x}_j$.

Solving Eq. 5 and Eq. 6, the Kriging weights are obtained as follows:

$$\boldsymbol{\lambda}^{\mathrm{T}} = \mathbf{p}^{\mathrm{T}}(\mathbf{x}_0)\left(\mathbf{P}^{\mathrm{T}}\mathbf{R}^{-1}\mathbf{P}\right)^{-1}\mathbf{P}^{\mathrm{T}}\mathbf{R}^{-1} + \mathbf{r}^{\mathrm{T}}(\mathbf{x}_0)\mathbf{R}^{-1}(\mathbf{I} - \mathbf{P}\mathbf{A}) \quad (10)$$

So, the Kriging estimate $u^h(\mathbf{x}_0)$ In Eq. 2 can be written as:

$$u^h(\mathbf{x}_0) = \mathbf{w}^{\mathrm{T}}\mathbf{d} \quad (11)$$

where:

d : $[u(\mathbf{x}_1) \quad \dots \quad u(\mathbf{x}_n)]^{\mathrm{T}}$= vector of the nodal point values.

Since a point $\mathbf{x}_0$ is any point in the DOI, it can be written as $\mathbf{x}$ and Eq. 11 changes to:

$$u^{\mathrm{h}}(\mathbf{x}) = \mathbf{N}(\mathbf{x})\mathbf{d} = \sum_{i=1}^{n} N_i(\mathbf{x})u_i \quad (12)$$

where $\mathbf{N}(\mathbf{x})$= $\mathbf{w}^{\mathrm{T}}(\mathbf{x})$ is the shape function matrix of the Kriging interpolation, that is,

$$\mathbf{N} = [N_1(\mathbf{x}) \quad N_2(\mathbf{x}) \quad \cdots \quad N_n(\mathbf{x})] \quad (13)$$

There are two main properties of the Kriging shape function that make it suitable for use in the finite element method, namely the Kronecker delta or interpolation and the consistency property (Gu, 2003; Plengkhom & Kanok-Nukulchai, 2005).

2.2 Polynomial Basis Function and Correlation Function

The polynomial basis function and a model of the covariance function are the forming functions of the Kriging shape function. The more the number of layers in the DOI, the higher the polynomial degree m. This is because the number of nodal points n in the DOI must be greater than or equal to the polynomial degree m. In this study, the maximum polynomial function used is of the third degree. In addition to polynomial functions, a pair of arbitrary variables can $U(\mathbf{x})$ be $U(\mathbf{x}+\mathbf{h})$ written in terms of the coefficient correlation function, or what is known as the correlation function.

The correlation function is written as follows (Wong & Kanok-Nukulchai, 2009):

$$\rho(\mathbf{h}) = C(\mathbf{h})/\sigma^2 \tag{14}$$

$$\sigma^2 = var[U(\mathbf{x})] \tag{15}$$

According to Gu (2003), the value σ^2 does not have a significant effect on the result, so the value of one will be used in this study. There are two kinds of correlation functions, namely Gaussian and Quartic Spline, that have been used in the Galerkin method or K-FEM (Gu, 2003; Dai *et al.*, 2003; Wong & Kanok-Nukulchai, 2006). The Gaussian function and the Quartic Spline (QS) function are given as follows, respectively:

$$\rho(\mathbf{h}) = e^{-(\theta\frac{h}{d})^2} \tag{16}$$

$$\rho(\mathbf{h}) = \begin{cases} 1 - 6\left(\theta\frac{h}{d}\right)^2 + 8(\left(\theta\frac{h}{d}\right)^3 - 3\left(\theta\frac{h}{d}\right)^4 & \text{untuk } 0 < \theta\frac{h}{d} < 1 \\ 0 & \text{untuk} \quad \theta\frac{h}{d} > 1 \end{cases} \tag{17}$$

where θ is the correlation parameters,h is the Euclidean distance between two nodes **x** and **x** + **h,** and d is the maximum distance between pairs of nodes in the DOI.

The lower and upper limits for the correlation parameter θ can be determined using the following criteria (Plengkhom & Kanok-Nukulchai, 2005):

$$|\sum_{i=1}^{n} N_i - 1| \leq 1\text{x}10^{-10+a} \tag{18}$$

$$\det(\mathbf{R}) \leq 1\text{x}10^{-b} \tag{19}$$

where:
a = order of the basis function (linear=1, quadratic =2, cubic = 3).
b = dimensional space of the problem.
Based on these criteria, Wong & Kanok-Nukulchai (2006) proposed the correlation parameter for application to K-FEM in the 2D domain as follows:

For the Gaussian correlation function, the parameter is given as

$$\theta = (1-f)\theta^l + f\theta^u, \ 0 \leq f \leq 0.8 \tag{20}$$

where f is the scale factor, the upper and lower limits are as follows:

$$\theta^l = \begin{cases} 0.08286n - 0.2386 & \text{for } 3 \le n < 10 \\ -8.364E-4n^2 + 0.1204n - 0.5283 & \text{for } 10 \le n \le 55 \\ 0.02840n + 2.002 & \text{for } n > 55 \end{cases} \quad (21)$$

$$\theta^u = \begin{cases} 0.34n - 0.7 & \text{for } 3 \le n < 10 \\ -2.484E-3n^2 + 0.3275n - 0.2771 & \text{for } 10 \le n \le 55 \\ 0.05426n + 7.237 & \text{for } n > 55 \end{cases} \quad (22)$$

For the QS correlation function, the parameter is given as

$$\theta = \begin{cases} 0.1329n - 0.3290 & \text{untuk } 3 \le \text{n} < 10 \\ 1 & \text{untuk } n \ge 10 \end{cases} \quad (23)$$

2.3 Domain of Influencing Nodes

The domain of the influencing nodes (DOI) is a layer of elements formed in a 2D domain that has been divided into a mesh of triangular elements. Each Kriging interpolation element is built based on a collection of nodes in the DOI. The Kriging interpolation function combines the interpolation of all elements in the domain so that the unknown global variables can be approximated.

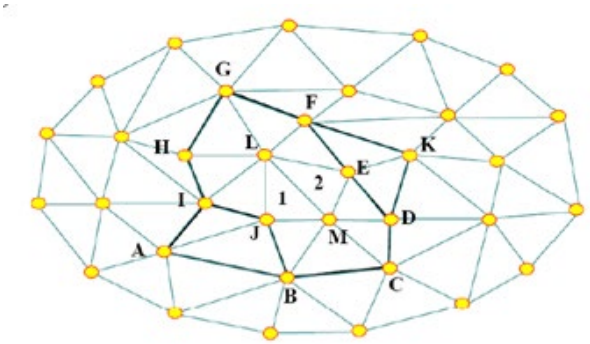

Figure 1. The DOI for element 1 and for element 2

Figure 1 illustrates the DOI concept. For example, there are two elements considered in this figure, namely Element 1 and Element 2. Let two layers of elements be selected as DOI for both elements. Element 1 forms the ABCDEFGHI polygon, and element 2 forms the BCDKFGHIJ polygon as the DOI. Element 1 includes 12 nodes for constructing Kriging interpolation, whereas Element 2 includes 11 nodes.

2.4 Elastodynamic

Plane stress is defined as a state of stress in a body (say, lying in the *x*-*y* plane) where the normal stress and shear stresses directed perpendicular to the plane, say in the *z*-axis, are negligible (Logan, 2016). The stress components acting on the plane stress model are shown in Fig. 2. The stress $\boldsymbol{\sigma}$ and strain $\boldsymbol{\varepsilon}$ matrices can be written as follows:

$$\boldsymbol{\sigma} = \begin{Bmatrix} \sigma_x \\ \sigma_x \\ \tau_{xy} \end{Bmatrix} \quad (24)$$

$$\boldsymbol{\varepsilon} = \begin{Bmatrix} \varepsilon_x \\ \varepsilon_x \\ \gamma_{xy} \end{Bmatrix} \quad (25)$$

The displacement in the *x*- an *y*-directions are functions of time t and can be written as

$$\mathbf{u} = \begin{Bmatrix} u(x,y,t) \\ v(x,y,t) \end{Bmatrix} \tag{26}$$

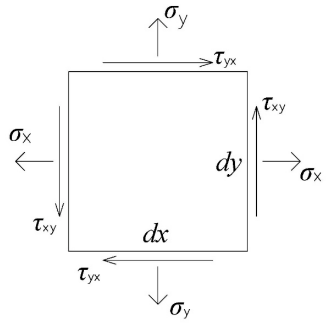

Figure 2. Stress components in a plane stress model

The normal stresses σ_x and σ_y that works on the model causes axial deformation measured by normal strains as follows:

$$\varepsilon_x = \frac{\partial u}{\partial x} \tag{27}$$

$$\varepsilon_y = \frac{\partial v}{\partial y} \tag{28}$$

The shearing stress τ_{xy} that works on the model causes shearing deformation, measured by shear strain follows:

$$\gamma_{xy} = \frac{\partial u}{\partial y} + \frac{\partial v}{\partial x} \tag{29}$$

In the matrix format, the relation is given as:

$$\begin{Bmatrix} \varepsilon_x \\ \varepsilon_y \\ \gamma_{xy} \end{Bmatrix} = \begin{bmatrix} \frac{\partial}{\partial x} & 0 \\ 0 & \frac{\partial}{\partial y} \\ \frac{\partial}{\partial y} & \frac{\partial}{\partial x} \end{bmatrix} \begin{Bmatrix} u \\ v \end{Bmatrix} \tag{30}$$

Or, briefly written as:

$$\boldsymbol{\varepsilon} = \boldsymbol{\partial}\, \mathbf{u} \tag{31}$$

By definition, other stress components are zero, that is,

$$\sigma_z = \tau_{xz} = \tau_{yz} = 0 \tag{32}$$

Using th Hooke's law, the constitutive plane stress equations are obtained as follows:

$$\boldsymbol{\sigma} = \mathbf{D}\, \boldsymbol{\varepsilon} \tag{33}$$

where matrices $\boldsymbol{\sigma}$ and $\boldsymbol{\varepsilon}$ are defined in Eq. 24 and Eq. 25, and

$$\mathbf{D} = \frac{E}{1+v^2} \begin{bmatrix} 1 & v & 0 \\ v & 1 & 0 \\ 0 & 0 & \frac{1-v}{2} \end{bmatrix} \tag{34}$$

where E is the modulus of elasticity and v is Poisson's ratio. This relationship can be derived from the 3D elasticity constitutive equation for an isotropic material model, that is,

$$\begin{Bmatrix} \sigma_x \\ \sigma_y \\ \sigma_z \\ \tau_{xy} \\ \tau_{yz} \\ \tau_{xz} \end{Bmatrix} = \frac{E}{(1+v)(1-2v)} \begin{bmatrix} 1-v & v & v & 0 & 0 & 0 \\ 0 & 1-v & v & 0 & 0 & 0 \\ 0 & v & 1-v & 0 & 0 & 0 \\ 0 & 0 & 0 & \frac{1-2v}{2} & 0 & 0 \\ 0 & 0 & 0 & 0 & \frac{1-2v}{2} & 0 \\ 0 & 0 & 0 & 0 & 0 & \frac{1-2v}{2} \end{bmatrix} \begin{Bmatrix} \varepsilon_x \\ \varepsilon_y \\ \varepsilon_z \\ \gamma_{xy} \\ \gamma_{yz} \\ \gamma_{xz} \end{Bmatrix} \tag{35}$$

Inserting Eq. (32) into Eq. (35) gives the **D** matrix in Eq. (34). The strain on direction z can be obtained as

$$\varepsilon_z = -\frac{v}{E}(\sigma_x + \sigma_y) \tag{36}$$

The equilibrium equation can be obtained by applying the second Newton's law to the free-body diagram, that is,

$$\frac{\partial \sigma_x}{\partial x} + \frac{\partial \tau_{xy}}{\partial y} + b_x = \rho \ddot{u} \tag{37}$$

$$\frac{\partial \tau_{xy}}{\partial x} + \frac{\partial \sigma_y}{\partial y} + b_y = \rho \ddot{v} \tag{38}$$

$$\tau_{xy} = \tau_{yx} \tag{39}$$

where b_x and b_y are the body force components in the *x*-axis and *y*-axis, respectively. Eq. 37 and Eq. 38 can be written in matrix from as follows:

$$\begin{bmatrix} \frac{\partial}{\partial x} & 0 & \frac{\partial}{\partial y} \\ 0 & \frac{\partial}{\partial y} & \frac{\partial}{\partial x} \end{bmatrix} \begin{Bmatrix} \sigma_x \\ \sigma_y \\ \tau_{xy} \end{Bmatrix} + \begin{Bmatrix} b_x \\ b_y \end{Bmatrix} = \begin{Bmatrix} \rho \ddot{u} \\ \rho \ddot{v} \end{Bmatrix} \tag{40}$$

$$\boldsymbol{\partial}^{\mathbf{T}} \boldsymbol{\sigma} + \mathbf{b} = \rho \ddot{\mathbf{u}} \tag{41}$$

Plane strain is defined as a strain state where the normal strain to the x-y plane, ε_z, and the the shear strains γ_{xz} and γ_{xz} are assumed to be zero. (Logan, 2016). The plain strain model has similarities with the plane stress model in the relations of the strain-displacement, equilibrium equation, and strain energy, whereas the stress-strain relation has the difference in the matrix **D**. In the plane strain model, by definition we can write:

$$\varepsilon_x = \gamma_{xz} = \gamma_{yz} = 0 \tag{42}$$

The matrix **D** for the plane strain model is

$$\mathbf{D} = \frac{E}{(1+v)(1-2v)} \begin{bmatrix} 1-v & v & 0 \\ v & 1-v & 0 \\ 0 & 0 & \frac{1-2v}{2} \end{bmatrix} \tag{43}$$

and normal stress in the direction z is given as:

$$\sigma_z = -v(\sigma_x + \sigma_y) \tag{44}$$

2.4.1 Weak Forms

The variational form of the governing equation for the plane strain and plane stress models

can be expressed as

$$\int_V \delta\boldsymbol{\varepsilon}^T\boldsymbol{\sigma}\, dV + \int_V \delta\ddot{\mathbf{u}}^T\rho\,\ddot{\mathbf{u}}\, dV = \int_V \delta\mathbf{u}^T\mathbf{b}\, dV + \int_S \delta\mathbf{u}^T\mathbf{t}\, dS \quad (45)$$

where $\mathbf{u} = \{u \quad v\}^T$ is the displacement vector, $\boldsymbol{\varepsilon} = \{\varepsilon_x \quad \varepsilon_y \quad \gamma_{xy}\}^T$ is the strain vector in the 2D plane, $\boldsymbol{\sigma} = \{\sigma_x \quad \sigma_y \quad \tau_{xy}\}^T$ is the stress vector in 2D plane, $\mathbf{b} = \{b_x \quad b_y\}^T$ is the body force vector, $\mathbf{t} = \{t_x \quad t_y\}^T$ is the traction force vector on the surface, and ρ is the mass density.

2.4.2 Weak Form Discretization

Let a 2D-domain Ω be divided into N_{el} elements and N nodes. The displacement vector $\mathbf{u} = \{u \quad v\}^T$ over a typical element is approximated using Kriging interpolation, as follows:

$$\mathbf{u}(x, y) \simeq \mathbf{N}\mathbf{d} \quad (46)$$

Here, the Kriging shape function matrix is defined as follows (not the same as in Eq. 13):

$$\mathbf{N} = \begin{bmatrix} N_1 & 0 & N_2 & 0 & \cdots & N_n & 0 \\ 0 & N_1 & 0 & N_2 & \cdots & 0 & N_n \end{bmatrix} \quad (47a)$$

and the nodal displacement vector is defined as (not the same as in Eq. 11)

$$\mathbf{d} = \{u_1 \quad v_1 \quad u_2 \quad v_2 \quad \ldots \quad u_n \quad v_n\} \quad (47b)$$

n : the number of nodes in the element DOI under consideration.

Using the usual finite element formulation (Cook *et al.*, 2002), the discrete equilibrium equation for the element is obtained as follows:

$$\mathbf{m}\ddot{\mathbf{d}} + \mathbf{k}\mathbf{d} = \mathbf{f} \quad (48)$$

where the element mass matrix $(2n \times 2n)$,

$$\mathbf{m} = \int_{V^e} \mathbf{N}^T\rho\mathbf{N}\, dV \quad (49)$$

The element stiffness matrix $(2n \times 2n)$,

$$\mathbf{k} = \int_{V^e} \mathbf{B}^T\mathbf{D}\mathbf{B}\, dV \quad (50)$$

and the element nodal force vector $(2n \text{ x } 1)$

$$\mathbf{f} = \int_{S^e} \mathbf{N}^T\mathbf{p}\, dS + \int_{V^e} \mathbf{N}^T\mathbf{b}\, dV \quad (51)$$

The integration is carried out over the element volume V^e and element side surfaces S^e.

The matrix $\mathbf{B}$ is the strain and displacement relationship matrix,

$$\mathbf{B} = \begin{bmatrix} N_{1,x} & 0 & N_{2,x} & 0 & \ldots & N_{ns,x} & 0 \\ 0 & N_{1,y} & 0 & N_{2,y} & \ldots & 0 & N_{ns,y} \\ N_{1,y} & N_{1,x} & N_{2,y} & N_{2,x} & \ldots & N_{ns,y} & N_{ns,x} \end{bmatrix} \quad (52)$$

The matrix $\mathbf{D}$ can be seen in Eq. 34 for a plane stress model and Eq. 43 for a plane strain model.

For triangular elements with area L and thickness h, Eq. 49 to Eq. 51 can be simplified to:

$$\mathbf{m} = \int_L \mathbf{N}^{\mathrm{T}} \boldsymbol{\rho} \mathbf{N}\, dA \tag{53}$$

$$\mathbf{k} = h \int_L \mathbf{B}^{\mathrm{T}} \mathbf{D} \mathbf{B}\; dA \tag{54}$$

$$\mathbf{f} = h \int_L \mathbf{N}^{\mathrm{T}} \mathbf{b}\; dA + h \int_{s^t} \mathbf{N}^{\mathrm{T}} \mathbf{t}\; ds \tag{55}$$

s^t: triangular element edge on which the traction force vector $\mathbf{t} = \{t_x \quad t_y\}^{\mathrm{T}}$ is applied to.

The global structural mass matrix $\mathbf{M}$ and the global stiffness matrix $\mathbf{K}$ can be obtained by assembling the element mass and stiffness matrices for all elements. The assembling process here involves the degree of freedom from the nodal points outside the element. For free vibration analysis, the global force vector **F** is taken to be a zero vector.

The natural frequencies and vibration modes of a model can be obtained from the eigen problem as follows (Yang *et al.*, 2016):

$$\mathbf{KD} = \lambda \mathbf{MD} \tag{56}$$

$$\lambda = \omega^2 \tag{57}$$

The value of natural frequency ω can be obtained from the characteristic equation of Eq. 56, viz.

$$\det([\mathbf{K}] - \omega^2[\mathbf{M}]) = 0 \tag{58}$$

Once the eigenvalues are obtained, the vibration mode shapes $\{\boldsymbol{\phi}_\mathbf{i}\}$ can be obtained from

$$\left([\mathbf{K}] - \omega_i^2[\mathbf{M}]\right)\{\boldsymbol{\phi}_\mathbf{i}\} = 0 \tag{59}$$

3. RESULTS AND DISCUSSIONS

3.1 Case Studies

The first case study is taken from Yang *et al.* (2016). The cantilever beam model of length *L* and height *D* is examined under the plane stress condition, as shown in Fig 3. The parameters used for the cantilever beam are *L* = 100 mm, *D* = 10 mm, *E* = 2.1×10^5MPa, Poisson's ratio *v* = 0.3, mass density $\rho = 8 \times 10^{-10}$kg/mm^3, and thickness *h*= 1 mm.

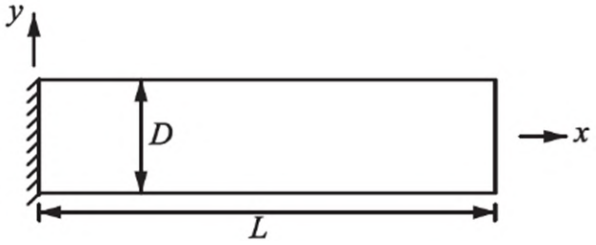

Figure 3. Cantilever beam

The second case study is taken from Wong, FT, & Syamsoeyadi, H. (2011), that is, a simply-supported beam as shown in Fig 4. The parameters used for the beam are *L* = 10 m, *h* = 2 m, *E* = 2×10^9N/mm ^{2,} *v* = 0.3, mass density ρ = 10kg/mm^3, and thickness b = 1 m.

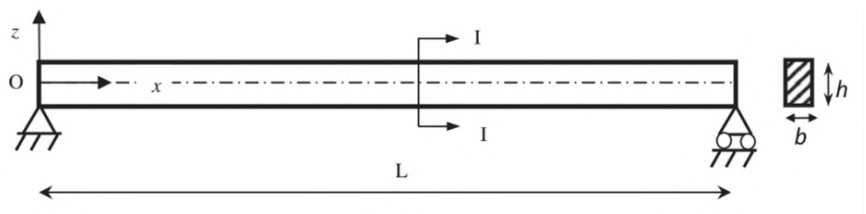

Figure 4. Simply-supporrted beam

The third case study is taken from Provatidis (2006), i.e, a thick arch model as shown in Fig. 5. The parameters used in the arch modeling are E/ρ =10 ^{4,}, v = 0.25, r_0 = 2.5 mm, and r_1 = 5 mm.

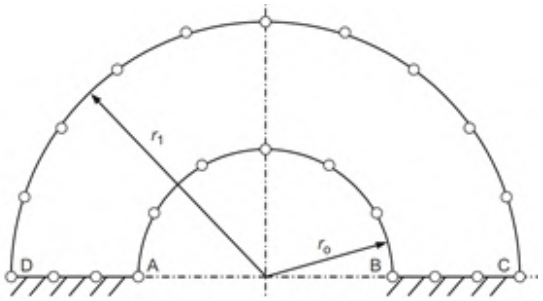

Figure 5. Thick arch

The fourth case study is taken from Yang *et al.* (2016), i.e., a shear wall with four holes as shown in Fig. 6. The parameters used in the shear wall are E = 1000 Pa, v = 0.2, mass density ρ=1 x 10^{-6}kg/m^3, and thickness h = 1 mm.

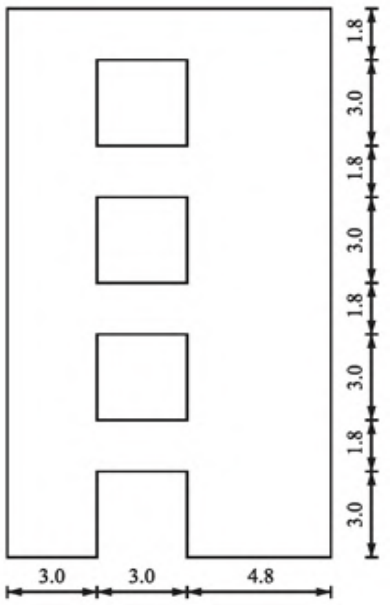

Figure 6. Shear wall with four holes

The fifth case study is taken from Yang *et al.* (2016), i.e., a slope as shown in Fig. 7. The parameters used in the slope model are E = 8x10^7 Pa, v = 0.43, and unit weight γ = 1.962 x 10^4N/m^3.

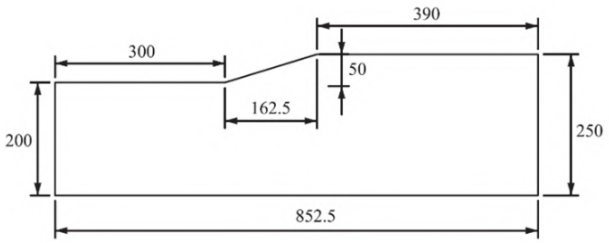

Figure 7. Slope model

The sixth case study is taken from Nguyen-Thanh *et al.* (2010), i.e., a tapered cantilever plate with a hole, as shown in Fig. 8. The parameters used for the tapered cantilever plate are E = 1 Pa, v = 0.3, ρ =1 kg/mm^3, r= 5 mm, and thickness h = 1 mm.

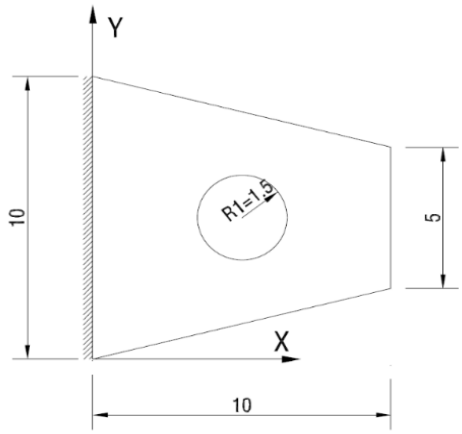

Figure 8. Tapered cantilever plate with a hole

3.2 Free Vibration Analysis Results

3.2.1 Cantilever Beam

The cantilever beam was analyzed using the plane-stress model. The analyses were carried out for different degrees of the polynomial basis (linear, quadratic, cubic) and different numbers of element layers for the DOI (1, 2, …, 5). The first eight natural frequencies of the cantilever beam obtained using meshes of 10×1, 20×2, and 40×4 Kriging-based elements are presented in Tables 1 to 3.

Table 1. Natural frequencies of the cantilever beam with a mesh of 10x1 Kriging-based elements

Linear					Reference
1	**2**	**3**	**4**	**5**	**Yang *et al.* (2016)**
1704	924	910	936	945	823
9550	5568	5463	5501	5485	4937
12899	12841	12849	12849	12853	12824
23636	14637	14271	14224	14105	13005
38879	26561	25759	25647	25572	23632
40961	38330	38477	38513	38567	36040
60075	40736	39424	39460	39451	38442
66226	56858	55236	54935	54481	49616

Table 2. Natural frequencies of the cantilever beam with a mesh of 20x2 Kriging-based elements

Linear					Quadratic			
1	**2**	**3**	**4**	**5**	**2**	**3**	**4**	**5**
1108	885	878	866	861	822	822	823	824
6551	5310	5248	5175	5143	4967	4980	5006	5026
12812	12804	12807	12806	12807	12795	12807	12807	12807
16992	13986	13808	13661	13617	13212	13270	13387	13463
30439	25384	25096	24937	24929	24247	24414	24678	24823
38511	38278	38304	38182	38222	37287	37635	38041	38213
45933	38690	38402	38386	38396	38359	38411	38388	38394
62757	52963	52791	52718	52802	51780	52287	52748	52873

Table 3. Natural frequencies of the cantilever beam with a mesh of 40x4 Kriging-based elements

Linear					Quadratic				Cubic	
1	**2**	**3**	**4**	**5**	**2**	**3**	**4**	**5**	**3**	**4**
907	842	834	829	829	823	823	823	823	823	823
5426	5053	5002	4974	4970	4946	4943	4943	4944	4939	4942
12833	12827	12828	12828	12828	12826	12827	12828	12828	12824	12826
14255	13319	13172	13101	13092	13052	13038	13034	13040	13021	13038
25853	24220	23929	23811	23799	23767	23730	23715	23733	23687	23735
38493	36958	36486	36322	36317	36317	36248	36211	36251	36160	36255
39399	38451	38459	38454	38456	38450	38459	38454	38456	38442	38450
54245	50910	50231	50026	50042	50096	49985	49914	49987	49828	49985

The corresponding mode shapes of the cantilever beam are shown in Fig. 9.

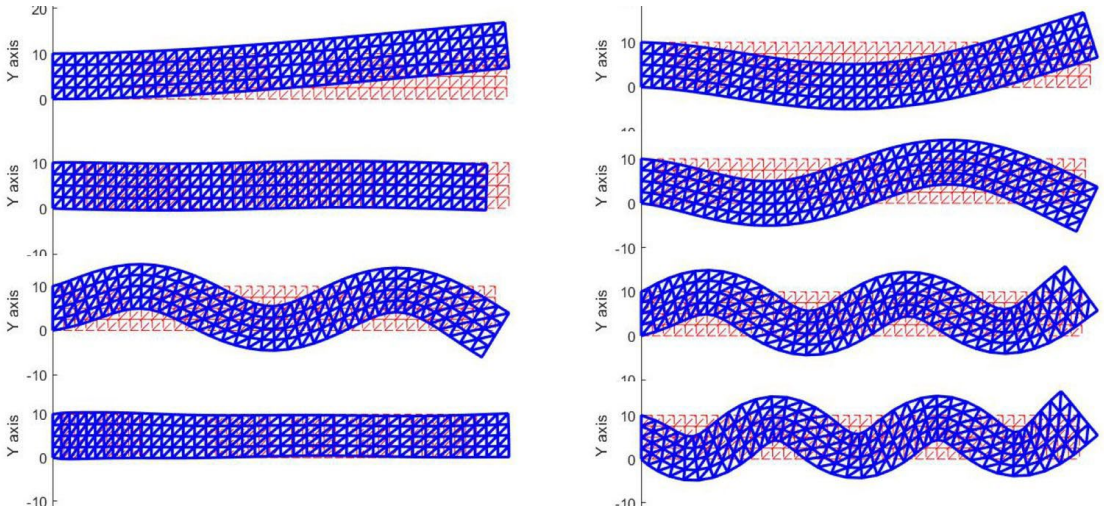

Figure 9. The first eight vibration modes of the cantilever beam

For the mesh size of 10×1, the K-FEM with quadratic and cubic polynomial bases cannot be applied; only the K-FEM with linear basis can work. Similarly, for the mesh size of 20×2, the K-FEM with cubic polynomial basis is not applicable. This is because the nodal points on the meshes are too few, so they cannot generate DOIs with enough element layers to construct Kriging shape functions with quadratic or cubic basis.

Tables 1 to 3 demonstrate that increasing the number of layers while using the same polynomial basis has little effect on the accuracy of the results. The exception is, of course, the K-FEM with linear basis, where increasing from one to two layers of DOIs significantly improves accuracy, particularly for the meshes of 10x1 and 20x2. This is because the K-FEM with a linear basis is essentially identical to the standard three-node triangular element, which is notable for its inaccuracy for a coarse or medium mesh size.

To examine the convergence of the natural frequencies with mesh refinement, the convergence graphs of the normalized natural frequencies computed using meshes of 10x1, 20x2, and 40x4 elements, with the K-FEM with linear and quadratic polynomial basis, are shown in Fig. 10. It is seen that the more the number of meshes, the closer the results to the reference values.

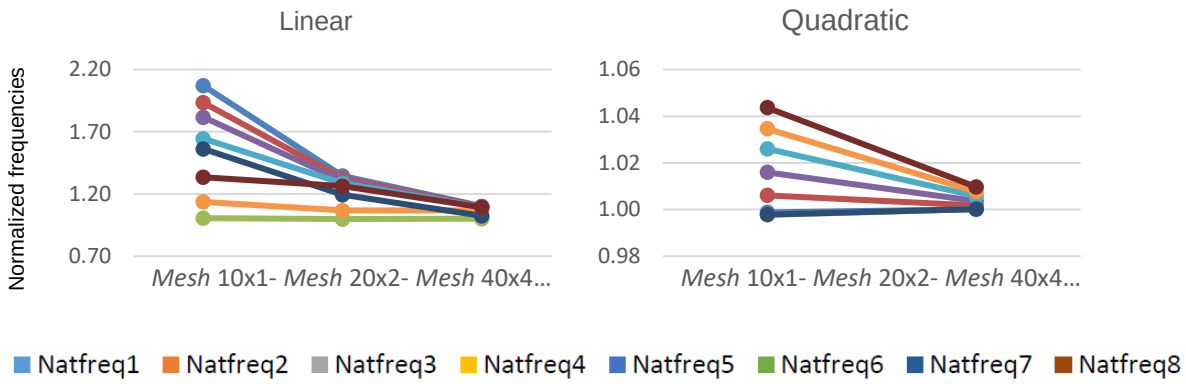

Figure 10. Convergence of normalized natural frequencies of the cantilever beam

It is noticed that the natural frequency results for the third mode are more accurate than the others. This is because the corresponding vibration mode is an axial deformation mode, which can be effectively captured even with the standard three-node triangular element.

3.2.2 Simply-Supported Beam

The simply-supported beam was analyzed using the plane-stress model. The first eight natural frequencies of the beam obtained using meshes of 10×1, 20×2, and 40×4 Kriging-based elements are presented in Tables 4 to 6. The corresponding mode shapes of the simply-supported beam can be seen in Fig. 11.

Regarding the applicable number of layers of DOIs used in the K-FEM in different mesh sizes, the explanation is the same as in the previous problem example. Morover, the findings in the previous problem can be shared here. The exception is that the results using the mesh size of 40×4 (Table 6), which are surprisingly lower than the reference values. A possible reason for this is that the reference solution used in this example is based on the Timoshenko beam model, whereas the beam in this analysis is modelled as the plane stress model.

Table 4. Natural frequencies of the simply-supported beam with a mesh of 10x1 elements

Linear					Reference Wong, FT, & Syamsoeyadi, H. (2011)
1	2	3	4	5	
3.24	2.50	2.50	2.51	2.51	2.29
6.56	5.30	5.35	5.38	5.38	5.10
7.22	7.01	7.04	7.06	7.08	7.06
10.60	8.29	8.38	8.43	8.44	8.35
14.40	11.37	11.65	11.84	11.89	11.90
15.03	13.51	13.74	13.88	13.92	14.00
19.75	14.83	15.73	16.17	15.90	15.65
21.94	18.26	19.85	20.22	19.69	19.60

Table 5. Natural frequencies of the simply-supported beam with a mesh of 20x2 elements

Linear					Quadratic			
1	2	3	4	5	2	3	4	5
2.74	2.53	2.53	2.52	2.50	2.34	2.38	2.39	2.42
6.06	5.65	5.64	5.61	5.59	5.36	5.47	5.52	5.57
7.07	7.04	7.05	7.05	7.06	7.03	7.05	7.06	7.06
9.97	9.25	9.25	9.20	9.20	8.91	9.15	9.24	9.31
14.14	13.06	13.13	13.08	13.11	12.72	13.20	13.30	13.35
14.20	13.93	14.00	14.01	14.02	13.88	14.01	14.03	14.03
18.64	17.00	17.22	17.20	17.30	16.75	17.55	17.61	17.59
21.24	20.47	20.68	20.71	20.75	20.31	20.73	20.78	20.79

Table 6. Natural frequencies of the simply-supported beam with a mesh of 40x4 elements

Linear					Quadratic			Cubic	
1	2	3	4	5	2	3	4	3	4
1.32	1.59	1.77	2.31	2.31	1.59	1.77	2.29	1.77	2.29
2.99	3.62	4.05	5.16	5.15	3.62	4.05	5.13	4.05	5.13
4.05	4.90	5.42	7.06	7.06	4.90	5.42	7.06	5.42	7.06
4.97	6.02	6.76	8.46	8.45	6.02	6.76	8.42	6.76	8.41
7.16	8.66	9.80	11.99	11.98	8.66	9.80	11.94	9.80	11.94
8.00	9.81	10.87	14.04	14.04	9.81	10.87	14.04	10.87	14.04
9.56	11.54	13.17	15.74	15.73	11.54	13.17	15.68	13.17	15.70
11.81	14.59	16.38	19.63	19.64	14.59	16.38	19.57	16.38	19.59

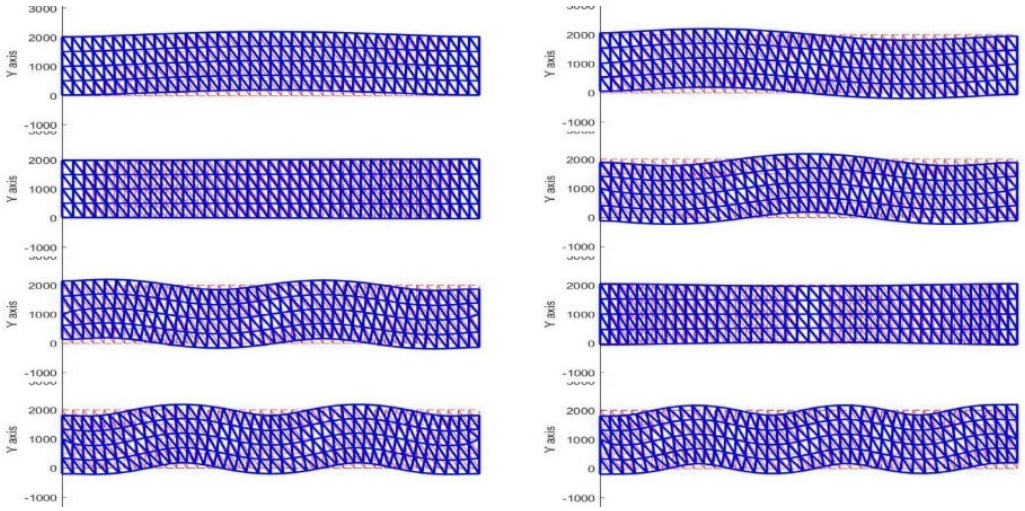

Figure 11. Eight vibration modes of the simply-supported beam

5.3 Thick Arch

The thick arch was analyzed using the plane-stress model. The resulting first four natural frequencies obtained using a mesh of 424 elements and 243 nodes are presented in Table 7. The reference natural frequency results are given in Table 8. The first eight mode shapes of the arch are shown in Fig. 12.

Table 7. Natural frequencies of the thick arch

Linear					Quadratic			Cubic	
1	**2**	**3**	**4**	**5**	**2**	**3**	**4**	**3**	**4**
2,291	2,274	2,263	2,263	2,263	2,264	2,258	2,260	2,254	2,256
3,389	3,368	3,357	3,358	3,357	3,362	3,355	3,357	3,355	3,355
5,251	5.219	5.204	5.205	5.204	5.211	5.202	5.204	5,200	5.201
5,817	5,760	5,728	5,728	5,726	5,738	5,720	5,723	5,713	5,715

Table 8. Reference natural frequency results for the thick arch

Reference Provatidis (2006)
2,242
3,346
5.191
5,688

Tables 7 and 8 show that the results are close to the reference values with a difference within 2% (except for the K-FEM with a linear basis and one-layer DOIs). This is because the mesh used has been sufficiently fine for computing the first eight natural frequencies.

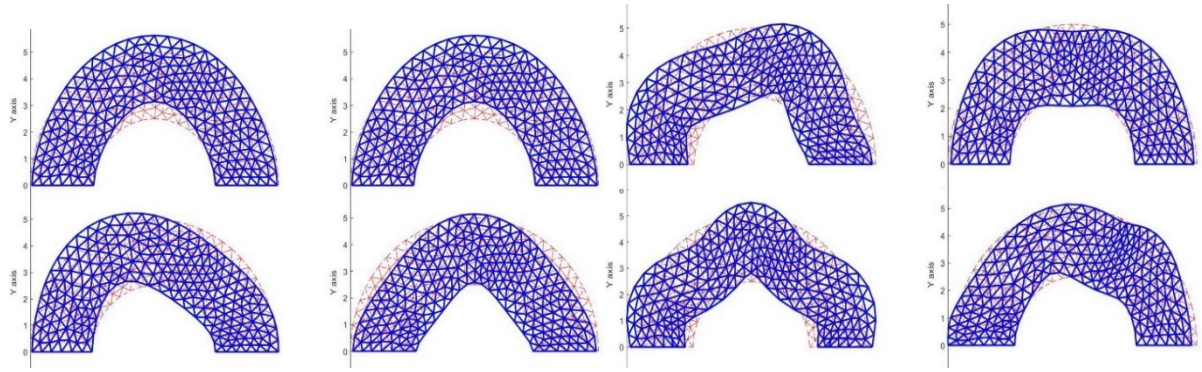

Figure 12. Eight vibration modes of the thick arch

5.4 Shear Wall with Four Holes

The shear wall was analyzed using the plane-stress model. Results for the first eight natural frequencies of the shear wall modelled with a mesh of 2608 elements and 1424 nodes are presented in Table 9. The reference natural frequency results are given in Table 10. The corresponding mode shapes of the shear wall are shown in Fig. 13.

Table 9. Natural frequencies of the shear wall

Linear					Quadratic			Cubic	
1	**2**	**3**	**4**	**5**	**2**	**3**	**4**	**3**	**4**
0.108	0.107	0.107	0.107	0.107	0.106	0.107	0.107	0.107	0.107
0.369	0.365	0.363	0.363	0.363	0.361	0.362	0.362	0.362	0.362
0.385	0.385	0.385	0.385	0.385	0.384	0.385	0.385	0.385	0.385
0.634	0.628	0.623	0.623	0.626	0.618	0.624	0.624	0.623	0.624
0.808	0.794	0.788	0.788	0.789	0.784	0.787	0.787	0.786	0.787
0.948	0.933	0.928	0.928	0.927	0.927	0.928	0.928	0.927	0.927
1,031	1012	1006	1006	1,004	1,004	1006	1006	1,004	1.005
1.146	1,134	1.128	1.128	1.126	1.125	1.127	1.127	1.126	1.126

Table 10. Reference natural frequency results for the shear wall

Reference Yang *et al.* (2016)
0.107
0.363
0.385
0.626
0.789
0.930
1008
1,130

Tables 9 and 10 demonstrate that all the results are very accurate. The maximum error is 1% for the ‘true’ K-FEM and 2% for the K-FEM with a linear basis and one-layer DOIs. These highly accurate results are achieved for the same reason as in the previous example.

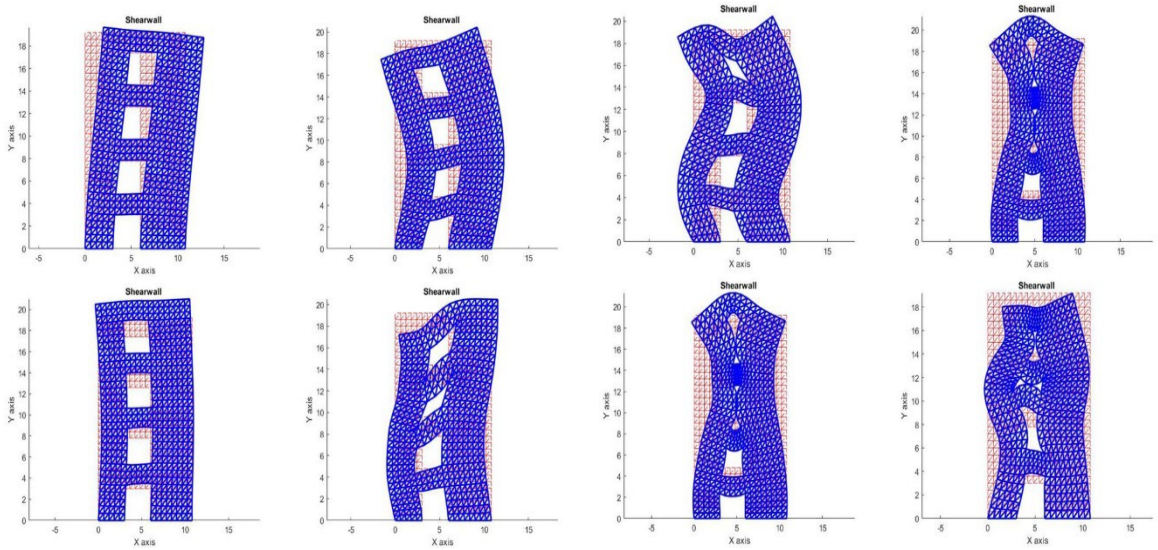

Figure 13. Eight vibration modes of the shear wall

5.5 Slope

The slope was analyzed with the plane-strain model. The resulting first eight natural frequencies of the slope, discretized with a mesh of 726 elements and 401 nodes, are presented in Table 11. The reference natural frequency results are presented in Table 12. The corresponding mode shapes of the slope are shown in Fig. 14.

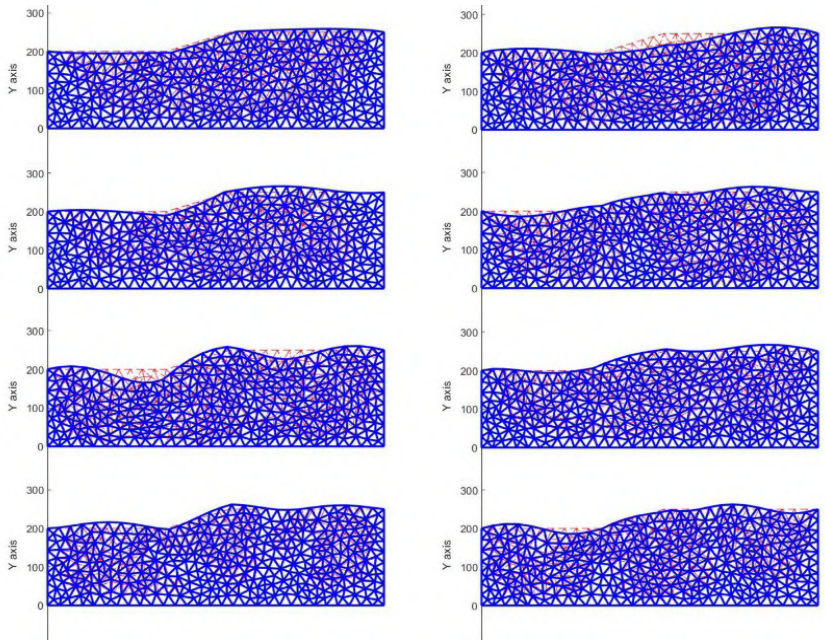

Figure 14. Eight vibration modes of the slope

Table 11. Natural frequencies of the slope

Linear					Quadratic			Cubic	
1	**2**	**3**	**4**	**5**	**2**	**3**	**4**	**3**	**4**
0.187	0.186	0.186	0.186	0.186	0.186	0.186	0.186	0.186	0.186
0.262	0.259	0.259	0.259	0.259	0.259	0.259	0.259	0.259	0.259
0.294	0.290	0.289	0.289	0.289	0.289	0.289	0.289	0.289	0.289
0.335	0.330	0.330	0.330	0.330	0.329	0.330	0.330	0.329	0.330
0.360	0.353	0.352	0.352	0.352	0.352	0.352	0.352	0.352	0.352
0.368	0.363	0.363	0.363	0.363	0.362	0.363	0.363	0.362	0.363
0.403	0.395	0.394	0.394	0.394	0.394	0.394	0.394	0.394	0.394
0.424	0.413	0.412	0.412	0.412	0.412	0.412	0.412	0.412	0.412

Table 1. Reference natural frequency results for the slope

References **Yang *et al.* (2016)**
0.179
0.240
0.276
0.307
0.313
0.357
0.358
0.383

Although a sufficiently fine mesh has been employed in the computations, the results are surprisingly quite different from the reference values (within 10% from the reference solution). A possible reason for the difference is a different value for the conversion from the given slope weight to the slope mass. In this study, we converted the unit weight into ρ = 1.962×10^3 kg/m^3 (assuming the value of g = 10 m/s^2).

5.6 Tapered Cantilever Plate with a Hole

The tapered cantilever plate was analyzed using the plane-stress model. Results of the first eight natural frequencies, obtained using a mesh of 624 elements and 354 nodes, are presented in Table 13. The reference natural frequency results are presented in Table 14. The corresponding mode shapes of the slope are shown in Fig. 15.

Table 2. Natural frequencies of the tapered cantilever plate

Linear					Quadratic			Cubic	
1	**2**	**3**	**4**	**5**	**2**	**3**	**4**	**3**	**4**
0.011	0.011	0.011	0.011	0.011	0.011	0.011	0.011	0.011	0.011
0.025	0.025	0.025	0.025	0.025	0.025	0.025	0.025	0.025	0.025
0.032	0.032	0.032	0.032	0.032	0.032	0.032	0.032	0.032	0.032
0.043	0.042	0.042	0.042	0.042	0.042	0.042	0.042	0.042	0.042
0.048	0.047	0.047	0.047	0.047	0.047	0.047	0.047	0.047	0.047
0.068	0.067	0.067	0.067	0.067	0.067	0.067	0.067	0.067	0.067
0.068	0.067	0.067	0.067	0.067	0.067	0.067	0.067	0.067	0.067
0.076	0.075	0.075	0.075	0.075	0.075	0.075	0.075	0.075	0.075

Table 3. Tapered cantilever plate references

References **Nguyen-Thanh *et al.*, (2010)**
0.012
0.026
0.033
0.047
0.052
0.070
0.071
0.079

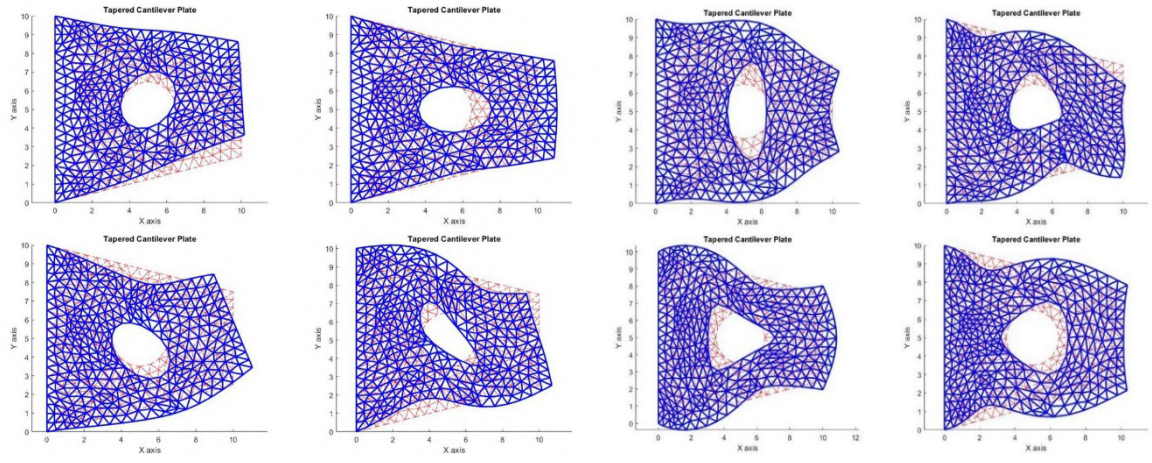

Figure 15. First eight vibration modes of the tapered cantilever plate

The results are surprisingly quite different from the reference values (the maximum difference is 11%), although a sufficiently fine mesh has been employed in the analysis. A possible reason for the difference is that the reference solution may have been analyzed using the plane strain approach, while in this case study, we use the plane stress model.

4. CONCLUSIONS

The K-FEM has been developed for free vibration analysis of plane stress and plane strain models. It has been tested on six plane elasticity free vibration problems, namely a cantilever beam, a simply-supported beam, an arch, a shear wall, a slope, and a tapered cantilever plate with a hole. The natural frequencies and mode shapes obtained using K-FEM show close agreement with reference solutions. Any discrepancies in the results arise from the differences in the input data used in the analysis with those used in the reference solution, rather than the limitations of the K-FEM itself.

High accuracy can be achieved even with moderate mesh refinement, and the results converge toward the reference values as the mesh is refined (*h*-refinement) or the degree of the polynomial basis increases (*p*-refinement). Increasing the number of DOI layers, however, has only a minor effect. A distinctive feature of K-FEM is that accuracy can be enhanced using the same mesh and the same number of global DOFs as the traditional FEM simply by raising the degree of its basis. These findings demonstrate that K-FEM is a viable and efficient method for practical free vibration analysis.

5. LIST REFERENCE

Cook, RD, Malkus, DS, Plesha, ME, & Witt, RJ (2002). *Concept and Applications of Finite Element Analysis.* Hoboken: John Wiley & Sons, Inc.

Coombs, WM, Charlton, TJ, Cortis, M., & Augarde, CE (2018). Overcoming volumetric locking in material point methods. *Computer Methods in Applied Mechanics and Engineering, 333,* 1-21.

Dai, KY, Liu, GR, Lim, KM, & Gu, YT (2003). Comparison between the radial point interpolation and the Kriging interpolation used in mesh-free methods. *Computational Mechanics, 32* (1), 60-70.

Gu, L. (2003). Moving Kriging interpolation and element-free Galerkin method. *International Journal for Numerical Methods In Engineering, 56* (1), 1-11.

Kim, NH (2014). *Introduction to Nonlinear Finite Element Analysis.* Springer Science & Business Media.

Lee, NS, & Bathe, KJ (1993). Effects of element distortions on the performance of isoparametric elements. *International Journal for Numerical Methods in Engineering, 36* (20), 3553-3576.

Logan, DL (2016). *A First Course in the Finite Element Method.* Cengage Learning.

Ludong, TA, Kentaro, C., & Wong, FT (2018). Triangle elements based on Kriging with continuous stress at nodal points (in Indonesian language). *Journal of Civil Engineering Dimension Pratama, 7* (1), 310-318.

Nguyen-Thanh, N., Rabczuk, T., Nguyen-Xuan, H., & Bordas, SP (2010). An alternative alpha finite element method (AαFEM) for free and forced structural vibration using triangular meshes. *Journal of computational and applied mathematics, 233* (9), 2112-2135.

Olea, RA (2012). *Geostatistics for Engineers and Earth Scientists.* Springer Science & Business Media.

Plengkhom, K., & Kanok-Nukulchai, W. (2005). An enhancement of finite element method with moving Kriging shape functions. *International Journal of Computational Methods, 2* (04), 451-475.

Provatidis, C. (2006). Free vibration analysis of two-dimensional structures using Coons-patch macroelements. *Finite elements in analysis and design, 42* (6), 518-531.

Wong, F. T., Widjaja, K & Soetanto, R. M. (2016). Studi keakuratan dan kekonvergenan metode elemen hingga berbasis kriging dan konvensional. *Prosiding Seminar dan*

Pameran HAKI, Jakarta, 23-24 Agustus 2016, Paper No. 25.

Wong, F. T., & Kanok-Nukulchai, W. (2006). Kriging-based finite element method for analyses of Reissner-Mindlin plates. *Proceedings of the Tenth East-Asia Pacific Conference on Structural Engineering and Construction*. Keynote Lectures and Symposia, Bangkok, 509-514.

Wong, FT, & Kanok-Nukulchai, W. (2009). On the convergence of the Kriging-based finite element method. *International Journal of Computational Methods, 6* (01), 93-118.

Wong, FT, & Syamsoeyadi, H. (2011). Kriging-based Timoshenko beam element for static and vibration-free analyses. *Civil Engineering Dimension, 13* (1), 42-49.

Yang, Y., Xu, D., & Zheng, H. (2016). Application of the three-node triangular element with continuous nodal stress for free vibration analysis. *Computers & Structures, 169,* 69-80.